ACS APPLIED BIO MATERIALS

www.acsabm.org Article

Photothermal Activatable Mucoadhesive Fiber Mats for On-Demand Delivery of Insulin via Buccal and Corneal Mucosa

Anna Voronova, Cristina Prieto, Maria Pardo-Figuerez, Jose Maria Lagaron, Amitav Sanyal, Bilal Demir, Thomas Hubert, Valerie Plaisance, Valerie Pawlowski, Séverine Vignoud-Despond, Alexandre Barras, Amar Abderrahmani, Rabah Boukherroub, and Sabine Szunerits*

Cite This: *ACS Appl. Bio Mater.* 2022, 5, 771–778 Read Online

ACCESS | Metrics & More | Article Recommendations | Supporting Information

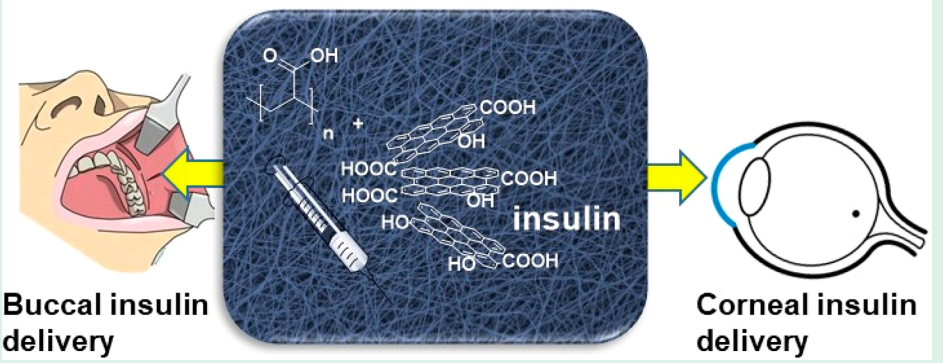

ABSTRACT: Electrospun fiber mats loaded with therapeutics have gained considerable attention as a versatile tool in the biomedical field. While these bandages are largely based on fast-dissolving polymers to release the cargo, stimuli-responsive fiber mats have the advantages of providing a timely and spatially controlled drug delivery platform, which can be refilled and reused several times. These benefits make electrospun fiber patches original platforms for painless and convenient on-demand hormone release. Because of the high need of more convenient and non-invasive methods for delivering insulin, a hormone that is currently used to treat hundred million people with diabetes worldwide, we have investigated the tremendous potential of reduced graphene oxide modified poly(acrylic acid) based fiber mats as an original platform for buccal and corneal insulin delivery on-demand. The PAA@rGO hydrogel-like fibers rendered water-insoluble by incorporating β-cyclodextrin, followed by thermal cross-linking, which showed adequate tensile strength along with high adsorption capacity of insulin at pH 7 and good recyclability. The fiber mats maintained good fibrous morphology and high loading efficiency even after five loading−release cycles. The mucoadhesive nature of the fibers allowed their application for insulin delivery via the eye cornea and the buccal mouth lining, as evidenced in *ex vivo* studies. Insulin loaded PAA@rGO hydrogel-like fibers showed an insulin flux via buccal lining of pigs of 16.6 ± 2.9 μg cm^{-2} h^{-1} and 24.3 ± 3.1 μg cm^{-2} h^{-1} for porcine cornea. Testing on healthy adult volunteers confirmed the excellent, mucoadhesive nature of the bandage, with three out of six volunteers feeling completely comfortable (note 8.3) while wearing the patches in the buccal cavity.

KEYWORDS: *electrospinning, on-demand release, reduced graphene oxide, mucoadhesive, buccal mucosa*

1. INTRODUCTION

Electrospinning of fiber mats incorporating therapeutic agents has become widely explored.[1−5] In contrast to other drug delivery systems, great flexibility can be achieved with these fiber mats.[6] While electrospun drug reservoirs have high drug loading capacity, drug delivery is guided by drug diffusion out of the matrix, as well as by the degradation/dissolution of the carrier polymer. A different concept is the controlled release of active principles at a certain time point, putting the patient into the center of action. One of the first example of the controlled release concept is linked to pH-sensitive electrospun stimuli-responsive fiber mats. Polymers with acid-labile functional groups as acetal and hydrazone groups can induce drug release at low pH.[7] While experimentally validated, the use of pH sensitive drug release from fiber mats for medical applications is currently limited to examples of treating inflamed issue.[8] On the other hand, temperature responsive fiber mats such as poly(*N*-isopropylacrylamide) (PNIPAM) are efficient drug loading matrixes at low temperature due increased porosity;

Received: November 13, 2021
Accepted: December 29, 2021
Published: January 13, 2022

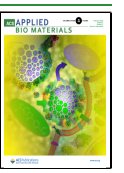

https://doi.org/10.1021/acsabm.1c01161
ACS Appl. Bio Mater. 2022, 5, 771−778

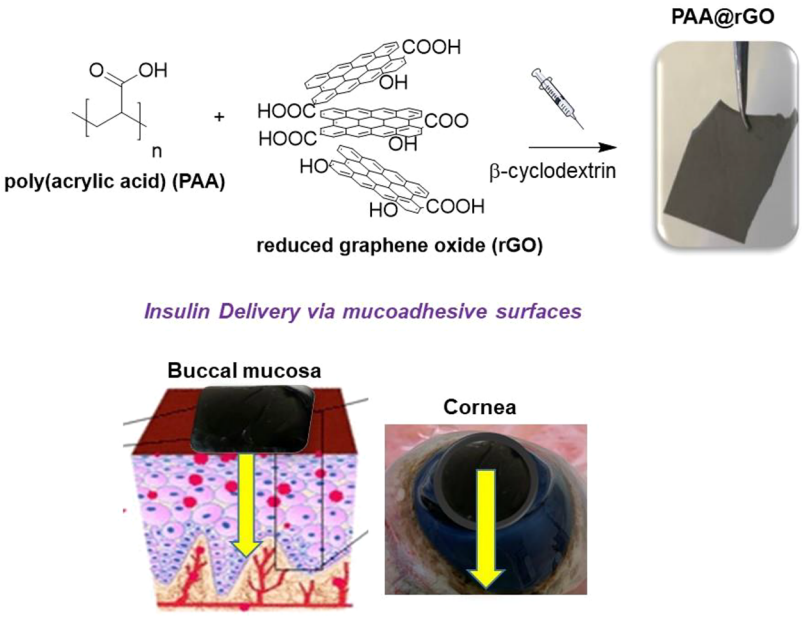

Figure 1. Illustration of the formation of PAA@rGO nanofiber mats using electrospinning method and their application for on-demand insulin release via mucoadhesive interfaces such as cornea and buccal mucosa. Ex vivo examples: cow cornea and pig buccal lining.

they are less adapted for temperature-controlled drug release in the form of external bandages on the human body. Electrospun fiber mats where an increase in temperature results in swelling of its 3D scaffold and drug release are more adapted for such applications. Some of us have demonstrated the utilization of reduced graphene oxide loaded poly(acrylic acid)-based hydrophilic nanofiber matrix for photothermal release of antibiotics. PAA was electrospun in the presence of beta-cyclodextrin (20 wt % of PAA) as a cross-linker. The formed PAA@rGO matrix features good photothermal heating properties reaching 51 ± 2 °C upon near-infrared irradiation at a power density of 1 W cm^{-1}. To widen the scope of this approach and investigate the feasibility of releasing macromolecular drugs, insulin was integrated and thermally released from PAA@rGO matrixes herewith.

The specific features of electrospun polymer fiber mats such as high surface-volume ratio and interconnected nonwoven architecture provide them with mucoadhesive properties and should be considered for transmucosal drug carrier systems.[9] In addition, transport of molecules across the buccal membrane, through less permeable than the sublingual area, is far simpler than the skin.[10] Skin, with a total thickness of about 2 mm, poses rate limiting barriers for drug diffusion via the *stratum corneum*. Buccal mucosal, on the other hand, is composed of mainly water (90−98%) and has a thickness of around 500 μm with characteristic pore sizes of ∼20−200 nm, making drug diffusion more likley. Mucoadhesive drug delivery is expected to improve drug bioavailability, to increase the patients' s therapy compliance, and to sustain drug delivery with a fast onset of action.[11,12] Being different from transdermal drug delivery route, mucosal surfaces are lacking the stratum corneum barrier, resulting in faster drug delivery. The inherent barriers for efficient buccal mucosal drug delivery are the keratinized tissue and the elimination of the drugs by the flashing action of saliva in the absence of unidirectional mucoadhesive mouth patches.[13]

We investigate, in this study, the usefulness of the PAA@rGO matrix as a mucoadhesive film for buccal linings and insulin release (Figure 1). We speculated that the presence of carboxyl groups in PAA and rGO together with hydroxyl groups of the cyclodextrin cross-linker ensures the interaction with the mucosal membrane. Indeed, results of mucoadhesive studies confirmed excellent muco-adhesion. *In vitro* and *ex vivo* insulin permeation studies using pig cheek lining and cow eyes demonstrated the possibility to deliver insulin via mucosal membranes opening new avenues for insulin therapy, which is so far based on subcutaneous insulin administration. Permeation studies using cow eyes and the photothermal fiber mat are investigated here as a model; in addition, the mucus layer covering the cornea is an important target to improve drug retention.[14]

2. RESULTS AND DISCUSSION

2.1. Characteristics of Mucoadhesive PAA@rGO Fiber Mats. Mucoadhesive patches were fabricated by electrospinning a mixture of PAA, β-cyclodextrin (20 wt % of PAA) and rGO (2.4 wt %). The bandages consist of a dense fiber mat (Figure 2a) with fibers of 400 ± 150 nm in diameter. Most importantly, PAA@rGO were water-insoluble and the fibrous nanostructures remained preserved even upon immersion in water for 1 week at 37 °C (Figure 2b). This contrasts with rGO-free PAA fibers which dissolve immediately after immersion in water. The PAA@rGO films proved to be also stable upon immersion into saliva (Figure 2c). This makes it different to others works for which the nanofiber film disintegration was initiated upon contact with stimulated salivary fluid in a time frame of about 150 s.[15]

Fiber mats assessed from four different batch fabrications had an average weight of 2.9 ± 1.3 mg and thickness of 120 ± 18 μm (Figure 2d). The degree of swelling was fast (Figure 2e), reaching up to 2000% of its weight in the first 30 s and a steady state after 1−2 min. Swelling was stronger in alkaline pH, with values reaching over 3000% for pH 9. The results of swelling behavior correlate with other works,[5] where the swelling ratio increased with increasing pH solution.

https://doi.org/10.1021/acsabm.1c01161
ACS Appl. Bio Mater. 2022, 5, 771−778

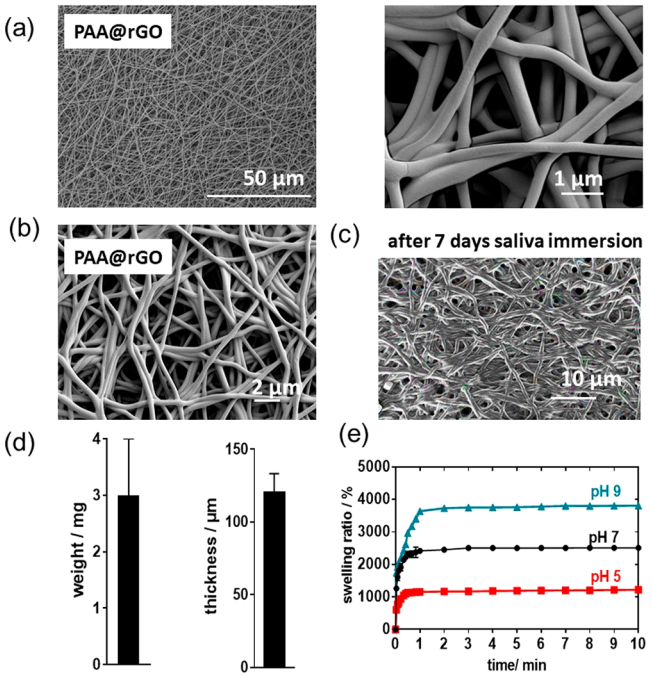

Figure 2. Characteristics of mucoadhesive PAA@rGO fiber mats: (a) SEM images at different magnifications. (b) SEM of PAA@rGO after immersion in water for 1 week at 37 °C. (c) Stability of the nanofiber film in salivary fluids. (d) Weight and thickness characteristics of four different batches of PAA@rGO. (e) Swelling behavior in water over time as a function of pH.

The presence of rGO was validated by the characteristic Raman bands at 1350 cm^{-1} (D-band) and 1580 cm^{-1} (G-band) (Figure 3a). The presence of rGO endows the mucoadhesive patch with photothermal properties (Figure 3b). Irradiation of PAA@rGO with a near-infrared laser (980 nm, 500 mW cm^{-2}) resulted in a surface temperature of 51 ± 2 °C within 5 min. The mechanical properties of PAA@rGO were also assessed, obtaining a measured mucoadhesive force of 0.74 (Figure 3c).[16,17]

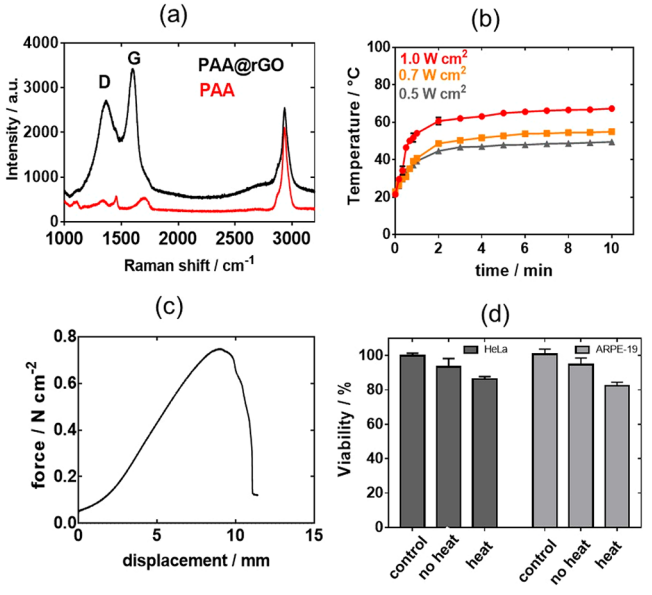

Figure 3. Characterization of PAA@rGO: (a) Raman spectra. (b) Photothermal heating curves at 980 nm illumination (0.5−1 W cm^{-2}). (c) Tensile tests via Force−displacement curve of PAA@rGO on porcine buccal mucosa. (d) Cell viability of ARPE-19 and HeLa cells in the presence of PAA@rGO without and with heat activation (0.5 W cm^{-2}, 10 min.).

The biocompatibililty of PAA@rGO mats was assessed on the HeLa and ARPE-19 cell lines (Figure 3d) using the resazurin assay. No loss in cell viability and metabolic activity was observed, suggesting the lack of residual monomers, which could lead to potential cytotoxicity. Thermal activation of the of PAA@rGO mats for 10 min at 500 mW cm^{-2} did also not show cell toxicity.

2.2. Insulin-Loaded Mucoadhesive PAA@rGO Patches. We opted for using insulin as a drug model, as this is the only drug option for treating patients with type 1 diabetes and the last option for patients with type 2 diabetes when the oral antidiabetic drugs have failed.[18] To decrease blood glucose concentrations, 250−330 nM (145−192 μg mL^{-1}) of insulin is needed. Human insulin (200 μg mL^{-1}) was consequently integrated into PAA@rGO fiber mats through their simple immersion for 3 h under continuous shaking at 4 °C. Insulin could be efficiently loaded (89% loading efficiency)[19] onto the mucoadhesive patches over a time span of 60 min (Figure 4a). These loading efficiencies are comparable to rGO loaded hydrogels (80%), as reported by some of us.[20] The loading capacity was pH-dependent with a higher loading at pH 4 (Figure 4a) due to insulin being positively charged and interacting with the negatively charged backbones of PAA@rGO fibers.

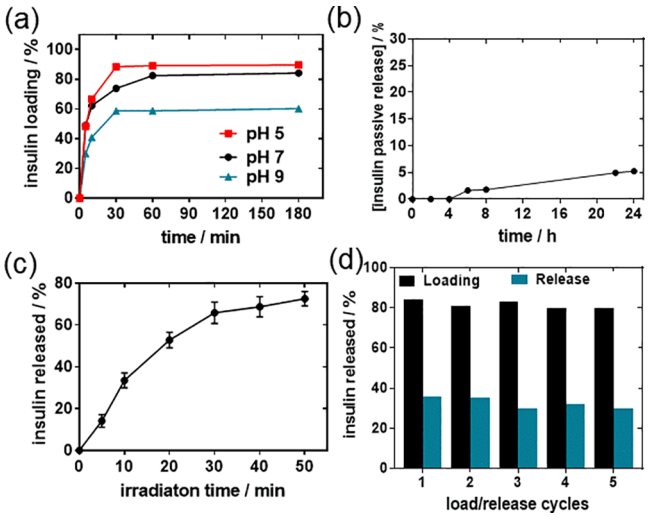

Figure 4. Insulin loaded PAA@rGO. (a) Human insulin (200 μg mL^{-1}) loading capacity. (b) Passive release over time. (c) Photothermal release with time (980 nm, 500 mW cm^{-2}). (d) Loading and release of insulin into the bandage.

To determine the amount of insulin passively and burst released from the mucoadhesive patch, the patch was immersed for 24 h in a solution of pH 7.4 (Figure 4b). Insulin was slowly released into the medium and was only detectable after 5 h immersion, mostly due to some insulin being trapped outside the patch. After 24 h, only 5% of insulin was released, correlating to 2.5 μg mL^{-1}. After conditioning of the patch, the remaining insulin was released on-demand upon photothermal activation (Figure 4c). The good heating capacity of the mucoadhesive patch results in an efficient heat triggered insulin release, reaching 150 μg (75%). Besides

https://doi.org/10.1021/acsabm.1c01161
ACS Appl. Bio Mater. 2022, 5, 771−778

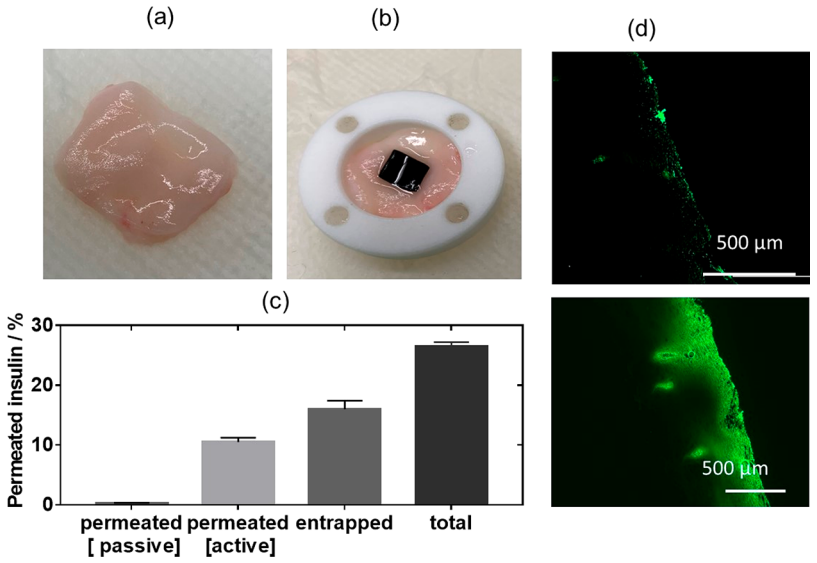

Figure 5. *Ex vivo* studies of insulin-loaded PAA@rGO nanofiber mats via porcine buccal mucosa: (a) Photographic image of porcine buccal tissue harvested and used for permeation studies. (b) Photograph of porcine buccal tissue fixed into Franz diffusion cell and immobilization of insulin-patch on top. (c) Cumulative permeation profile of insulin through the buccal tissue after 6 h upon passive or photothermal activation (10 min action with laser at 980 nm, 500 mW cm^{-2}) (n = 3). Error bars represent standard error of the mean (SEM) (d) Fluorescence images of buccal tissue treated with a FTIC-insulin loaded PAA@rGO patch without (top) and with (10 min, 980 nm, 500 mW cm^{-2}) activation (bottom).

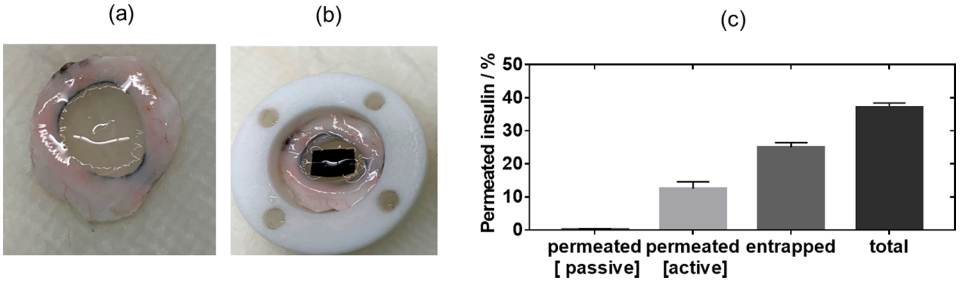

Figure 6. *Ex vivo* insulin permeation studies of insulin-loaded PAA@rGO nanofiber mats via porcine cornea: (a) Photographic image of porcine buccal tissue harvested and used for permeation studies. (b) Photograph of porcine buccal tissue fixed onto Franz diffusion cell and immobilization of insulin-patch on top. (c) Cumulative permeation profile of insulin through porcine cornea after 24 h upon passive or photothermal activation (10 min irradiation at 980 nm, 500 mW cm^{-2}) (n = 3). Error bars represent standard error of the mean (SEM).

the sufficient photothermal release, PAA@rGO fiber mats featured appropriate reusability. Reloading of the mats with insulin followed by photothermal activation for 10 min could be performed with the same efficacy for 5 successive cycles.

2.3. Ex Vivo Insulin Permeation Analysis. The distinct keratinization of the oral mucosa negatively impacts on the passage of drugs through the mucosa and limits therapeutic efficiency.[21] The absorption of insulin (Figure 5a) was determined by *ex vivo* permeability studies using pig buccal mucosa.[17,22] To determine the permeability of insulin, a patch of electrospun fibers (1.5 × 1.5 cm^2, 2 mg) was loaded with 500 $\mu g\ mL^{-1}$ of insulin by immersion into 1 mL solution at 4 °C for 1 h. With a loading efficiency of 82% (Figure 4a), this accounts for 410 $\mu g\ mL^{-1}$ of insulin integrated to the patch. This patch was placed on the top of the porcine buccal mucosa (Figure 5b) and both passive and heat-initiated permeations of insulin were assessed (Figure 5c). As expected, without heat activation, the insulin-loaded fiber mat showed limited insulin permeation through the epithelial cells of the porcine mucosa. In contrast, photothermal laser activation for 10 min resulted in substantial insulin penetration across the buccal tissue. After 6 h, 12 ± 2% of insulin (which accounts for 41.1 $\mu g\ mL^{-1}$ insulin) has permeated the porcine mucosa model, with about 16 ± 1% of insulin having been detected in the porcine lining. In total, the patches activated by heat were able to transport 28 ± 2% (82 $\mu g\ mL^{-1}$) of the loaded insulin into the buccal lining. These findings are in line with recently reported buccal patches by Vaidya and Mitragotri.[17] With a flux of 16.6 ± 2.9 $\mu g\ cm^{-2}\ h^{-1}$ insulin, the approach outperforms skin-based approaches.[20] It is comparable with results by some of us using an electrothermal activation approach (J = 15.6 ± 1.3 $\mu g\ cm^{-2}\ h^{-1}$)[19] and in line with insulin delivered from poloxamer-407 gels.[23] As the buccal mucosa is deficient of a stratum corneum layer, insulin can pass unhindered into the entire buccal epithelium. Fluorescence analysis of harvested buccal tissue before and after heat treatment and delivery of FITC-label insulin (Figure 5d) showed no structural damage of the tissue at the application site with the fluorescence signal remaining localized in the tissue without heat application. After 10 min heat application and observing the fluorescence stained tissue after 6 h, fluorescence of 500 μm in depth was observed, equal to the thickness of buccal nonkeratinized structures, The increased temperature might induce a mucus thinning effect and the protective role of PAA@GO against saliva proteases could be the reasons for the efficient insulin delivery.

https://doi.org/10.1021/acsabm.1c01161
ACS Appl. Bio Mater. 2022, 5, 771−778

In addition, comparable experiments were performed on pig cornea (Figure 6a,b). Permeation of insulin via the pig cornea was comparable to that of pig buccal mucosa, with limited passive diffusion; 13 ± 1% of insulin permeated the cornea and 25 ± 1% remained on the cornea tissue after 6 h, corresponding to a total insulin of 37 ± 1%, that is, 151 ± 3 μg mL^{-1} and an insulin flux of 24.3 ± 3.1 μg cm^{-2} h^{-1} (Figure 6b). This flux is several-times larger than that achieved using photothermal activation via porcine skin and 1.5 times using buccal mucosa.

2.4. *In Vivo* Mucoadhesive Properties of PAA@rGO Nanofiber Mats. Pancreatectomized Gottingen minipigs are valuable models of insulin-dependent diabetes as they share many similarities with humans such as the morphology of the pancreas and the overall metabolic status of the two species.[25] To investigate the efficiency of the nanofiber mat to lowerblood glucose level (BGL), insulin (100 μg mL^{-1} corresponding to 2.88 Insulin units) was loaded into the PAA@rGO fibers and applied inside the buccal cavity of the pig (Figure 7a). After thermal activation of the fiber mats for 10 min, the buccal lining (after removal of the insulin-loaded PAA@rGO fiber mat) showed no irritation and visual degradation (Figure 7b). Thermal activation of the fiber mats for 10 min resulted in an immediate reduction of the BGL (Figure 7c), while the BGL remained constant over the same time period without thermal activation (control experiment). The decrease of the BGL agrees with an increase in the plasma insulin concentration, with a maximum after 45 min (Figure 7c). Statistical evaluation using the 2-way ANOVA test of the BGL results (Figure 7c) indicated that after 15 min, the BGL after thermal activation is significantly different from the control (Figure 7d).

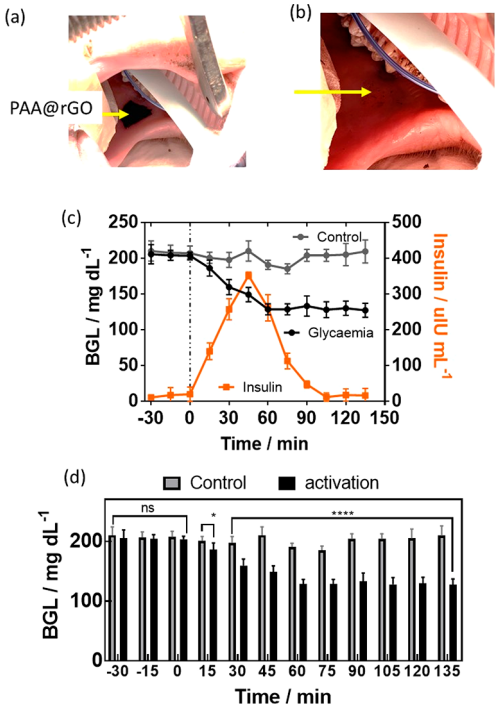

Figure 7. *In vivo* permeation study of insulin from PAA@rGO fiber mats via the buccal lines of mini-Pigs: (a) Image of pig buccal cavity in the presence of the PAA@rGO fiber mat. (b) Image of buccal cavity after photothermal activation for 10 min (500 mW cm^{-2}) and removal of PAA@rGO fiber mat. (c) Effect of insulin (2.88 IU) loaded PAA@rGO fiber mats on blood glucose level (BGL) over time after thermal activation (10 min irradiation at 980 nm, 500 mW cm^{-2}) (black) and with no heat activation (gray) together with time dependent blood insulin level in minipig (orange). (n = 3). Error bars represent standard error of the mean (SEM) (d) Statistical evaluation of BGL results (Figure 7c). 2-way ANOVA test with 99% confidence: n.s. (not significant), p < 0.01 (*), p < 0.0001 (****).

2.5. Acceptability of PAA@rGO Nanofiber Mats by Volunteers. Finally, we applied PAA@rGO nanofiber mats to 6 adult volunteers (three male, three female) between 25 and 49 years old (Figure 8a). The adhesion evaluated for a time span of 120 min was excellent, with all bandages residing for 120 min in the six cases (Figure 8b). The volunteers rated the patch as excellent (note of 9.3) with most of volunteers feeling comfortable (note 8.3) while wearing the patches in the buccal cavity. Two male volunteers considered it "mentally" difficult to have a nanomaterial in the mouth and the discomfort was related to this rather than the bandage itself. All volunteers agreed that the patches had no taste (note 10). The rating for removing the bandage is evaluated as medium (note of 6.1). None of them reported interference with speak nor effects on saliva production and swallowing.

3. CONCLUSION

In summary, it was shown that the incorporation of reduced graphene oxide into water insoluble fiber mats, formed from poly(acrylic acid) and β-cyclodextrin cross-linker by electrospinning, leads to the formation of water insoluble hydrogels with good photothermal characteristics. The resulting hydrogel fiber mat allowed efficient loading of a therapeutic peptide like insulin, while maintaining its good fibrous morphology. Using porcine buccal mucosa as well as porcine cornea as *ex vivo* models, the flux of insulin across the mucosal lining recorded upon passive or photothermal activation was investigated. As in the case of previously reported photothermal transdermal insulin delivery, thermal activation resulted in strongly increased insulin permeation rates reaching J = 16.6 ± 2.9 μg cm^{-2} h^{-1} for buccal mucosa and J = 24.3 ± 3.1 μg cm^{-2} h^{-1} for porcine cornea, being several times more elevated than transdermal delivery. This result confirms that buccal mucosa is suitable for the non-invasive delivery of insulin via electrospun fiber mats-based mucoadhesive patches. Efficient release of insulin by photothermal activation supports the idea of using mucoadhesive patches containing insulin for treating patients with diabetes. In type 2 diabetes, the most prominent form of diabetes, oral medication, is often supplemented by basal insulin therapy. In general, this biotherapy does not require a high dose of insulin. The quantity of insulin released from the herein presented mucoadhesive patches could be in line with their use in basal therapy. Therefore, compared to multiple insulin injection, this mode of delivery offers a huge advantage by increasing the compliance of patients to treatment, as it is resilient and can be easily self-administrated. In this perspective, our study allows future preclinical studies aiming to test the efficiency of this original platform to on-demand deliver insulin and to treat diabetes in animal models of diabetes. In addition, the proposed local insulin delivery system can be converted to a blood glucose concentration responding matrix via the integration of boronic acid surface ligands and might further widen the general concept of the work outlined here.

https://doi.org/10.1021/acsabm.1c01161
ACS Appl. Bio Mater. 2022, 5, 771−778

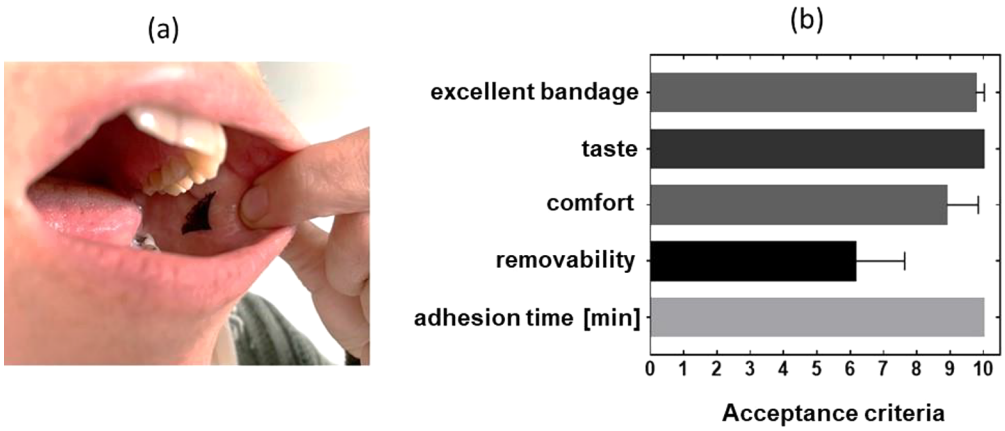

Figure 8. *In vivo* mucoadhesive performance of PAA@rGO nanofiber mats placebo: (a) Photograph of placement of mucoadhesive patches in humans attached by 5 s pressure application. (b) Acceptability evaluation of six adult volunteers on the adhesion time, overall bandage excellence, comfort, taste, and removability, in a scale of 0 (bad)-5 (medium)-10 (excellent); in terms of tast 0 indicates bad taste and 10 indicates no taste.

4. EXPERIMENTAL SECTION

4.1. Materials. Polyacrylic acid (PAA, Mn 450 000 g mol^{-1}), β-cyclodextrin, recombinant insulin, insulin FITC, artificial saliva, phosphate-buffered saline (PBS, pH 7.4) were purchased from Sigma-Aldrich. Reduced graphene oxide (rGO) in powder form was purchased from Graphenea (Spain).

The electrospinning of nanofiber mats was performed in a high-throughput electrospinning equipment Fluidnatek® LE 100 from Bioinicia S.L (Spain) according to a modified procedure described by us previously (See SI S1).[24]

Characterization methods are described in SI S2.

4.2. Determination of Swelling Degree, Weight, Thickness, and Cytotoxicity. The nanofiber mat was cut into smaller pieces (1 × 1 cm), dried (70 °C, 24 h) before weighting. The dried samples were then dipped into water at room temperature for 1 h and taken off at given time intervals (2 s to 10 min). The nanofiber pieces were dried with a cotton tissue in order to remove any remaining water and weighted using a microbalance. The swelling ratio of nanofiber mats was calculated as following:

$$\text{swelling degree}(\%) = \frac{W_t - W_d}{W_d} \times 100$$

where W_t is the weight of wet nanofibers at time t and W_d is the weight of dry nanofibers.

The measurements of weight, thickness and pH were performed in triplicates. The thickness was determined using a thickness gage ID-C112XBS from Mitutoyo Corporation (Japan). For weight determination, the mats of 1 × 1 cm^2 in size were weighted on a digital balance. The pH value was determined with a pH meter by immersion of the nanofiber mats into water for 2 min.

For experimental details of cytotoxicity tests of PAA@rGO bandage see SI S3.

4.3. Drug Loading and Release Studies. Insulin-FITC and insulin loaded patches were produced by immersion of 3.0 ± 1.0 mg PAA@rGO electrospun mats into 1 mL (200 μg mL^{-1}) of insulin-FITC or insulin aqueous solutions under continuous shaking at 150 rpm for 4 h at 4 °C.

In vitro photothermal drug release is described in SI S4).

Ex vivo permeation experiments are detailed in SI S5.

4.4. In Vivo Experiments Using Mini-Pigs. Insulin delivery in vivo was tested on female domestic pigs (three) weighing 50−62 kg. The animals were subjected to total pancreatectomy a day before each experiment. The insulin loaded patches (2.8 IU) were placed inside the buccal lining of the pig mouth. No fixing is needed due to the excellent mucoadhesive character of the patch. The PAA@rGO patch was activated for 10 min to reach a temperature of ∼50 °C. Glucose levels were measured directly from fresh blood via central catheter using a commercial glucometer. Blood samples were centrifuged at 5,000 rpm for 10 min at 4 °C and plasma was immediately separated and stored at −80 °C. Insulin concentrations were determined with Bi-Insulin RIA, France. All the manipulations in pigs, including total pancreatectomy, placing of the catheter, microneedles and patch activation as well as blood samplings, were performed under general anesthesia with a 2−3% concentration of isoflurane (Aerrane; Baxter, France) and under analgesia with transcutaneous fentanyl (Recuvyra; Elanco; France). Animal studies were approved by via protocol no. 21080 and performed in accordance with the guidelines for animal use specified by the European Union Council Directive of September 22, 2010 (2010/63/EU).

4.5. In Vivo Residence Times. The residence time was evaluated on six volunteers (three males and three females). Placebo patches (15 × 12 mm) were used and the residence time was 2 h. An acceptable questionnaire was filed by each volunteer to obtain information about taste, comfort, dry mouth, and salivation.

■ ASSOCIATED CONTENT

Supporting Information

The Supporting Information is available free of charge at https://pubs.acs.org/doi/10.1021/acsabm.1c01161.

Experimental details of electrospinning process (S1). Characterization methods and instruments used (S2). Details on cytotoxicity tests of PAA@rGO bandage (S3). In vitro photothermal drug release conditions (S4). Details on ex-vivo permeation experiments (S5) (PDF)

■ AUTHOR INFORMATION

Corresponding Author

Sabine Szunerits − *Univ. Lille, CNRS, Centrale Lille, Univ. Polytechnique Hauts-de-France, UMR 8520-IEMN, F-59000 Lille, France;* orcid.org/0000-0002-1567-4943; Phone: +33 (0)3 62 53 17 25; Email: sabine.szunerits@univ-lille.fr

Authors

Anna Voronova − *Univ. Lille, CNRS, Centrale Lille, Univ. Polytechnique Hauts-de-France, UMR 8520-IEMN, F-59000 Lille, France*

Cristina Prieto − *Institute of Agrochemistry and Food Technology (IATA), Spanish Council for Scientific Research (CSIC), 46980 Paterna, Spain;* orcid.org/0000-0002-0925-896X

https://doi.org/10.1021/acsabm.1c01161
ACS Appl. Bio Mater. 2022, 5, 771−778

Maria Pardo-Figuerez − *Institute of Agrochemistry and Food Technology (IATA), Spanish Council for Scientific Research (CSIC), 46980 Paterna, Spain*
Jose Maria Lagaron − *Institute of Agrochemistry and Food Technology (IATA), Spanish Council for Scientific Research (CSIC), 46980 Paterna, Spain;* orcid.org/0000-0002-0502-359X
Amitav Sanyal − *Department of Chemistry, Bogazici University, Bebek 34342 Istanbul, Turkey;* orcid.org/0000-0001-5122-8329
Bilal Demir − *CEA-TECH Region, Department Hauts-de-France, 59000 Lille, France*
Thomas Hubert − *University Lille, CHU Lille, European Genomic Institute of Diabetes (EGIDE), INSERM, Institut Pasteur Lille, UMR 1190, F-59000 Lille, France*
Valerie Plaisance − *Univ. Lille, CNRS, Centrale Lille, Univ. Polytechnique Hauts-de-France, UMR 8520-IEMN, F-59000 Lille, France*
Valerie Pawlowski − *Univ. Lille, CNRS, Centrale Lille, Univ. Polytechnique Hauts-de-France, UMR 8520-IEMN, F-59000 Lille, France*
Séverine Vignoud-Despond − *LETI-DTBS, CEA, 38054 Grenoble, France*
Alexandre Barras − *Univ. Lille, CNRS, Centrale Lille, Univ. Polytechnique Hauts-de-France, UMR 8520-IEMN, F-59000 Lille, France;* orcid.org/0000-0003-2821-7079
Amar Abderrahmani − *Univ. Lille, CNRS, Centrale Lille, Univ. Polytechnique Hauts-de-France, UMR 8520-IEMN, F-59000 Lille, France*
Rabah Boukherroub − *Univ. Lille, CNRS, Centrale Lille, Univ. Polytechnique Hauts-de-France, UMR 8520-IEMN, F-59000 Lille, France*

Complete contact information is available at: https://pubs.acs.org/10.1021/acsabm.1c01161

Author Contributions

The manuscript was written through contributions of all authors.

Notes

The authors declare no competing financial interest.

■ ACKNOWLEDGMENTS

The Centre National de la Recherche Scientifique (CNRS), the University of Lille, the Hauts-de-France region, and the CPER "Photonics for Society" are acknowledged for financial support. This work was partly supported by the French Renatech network. A.V. thanks the i-SITE foundation of the University of Lille for a PhD fellowship. This project has received funding from the European Union's Horizon 2020 Research and Innovation Staff Exchange (RISE) Marie Skłodowska-Curie Actions under grant agreement No 690836. We acknowledge the help and involvement of the Dhure (Département Hospitalo-Universitaire de Recherche et d'Enseignement) platform in work related to the mini-pig.

■ REFERENCES

(1) Huang, C.; Soenen, S. J.; Rejman, J.; Licas, B.; Braeckmans, K.; Demeester, J.; De Smedt, S. C. Stimuli-responsice electrospun fibers and their applications. *Chem. Soc. Rev.* **2011**, *40*, 2417−2434.
(2) Celebioglu, A.; Uyar, T. Hydrocortisone/cyclodextrin complex electrospun nanofibers for a fast-dissolving oral drug delivery system. *RSC Med. Chem.* **2020**, *11*, 245−258.
(3) Topuz, F.; Uyar, T. Electrospinning of cylodextrin functinal nanobibers for Drug delivery applications. *Pharmaceutics* **2019**, *11*, 6.
(4) Xue, J.; Wu, T.; Dai, Y.; Xia, Y. Electrospinning and Electropsun Nanobifers: Methods, materials, and applications. *Chem. Rev.* **2019**, *119*, 5298−5415.
(5) Li, L.; Hsieh, Y.-L. Ultra-fine polyelectrolyte fibers from electrospinning of poly(acrylic acid). *Polymer* **2005**, *46*, 5133−5139.
(6) Ning, Y.; Shen, W.; Ao, F. Application of blocking and immobilization of electrospun fiber in the biomedical field. *RSC Adv.* **2020**, *10*, 37246−37265.
(7) Cao, S.; Hu, B.; Liu, H. Synthesis of pH-responsive crosslinked poly[styrene-co-(maleic sodium anhydride)] and cellulose composite hydrogel nanofibers by electrospinning. *Polym. Int.* **2009**, *58*, 545.
(8) Wallace, L. A.; Gwynne, L.; Jenkins, T., Challenges and opportunities of pH in chronic wounds *Therap. Deliv.* 2019, *10*.
(9) Sofi, H. S.; A, A.-h.; Ivanovski, S.; Zhang, Y. S.; Sheikh, F. Electrospun nanofibers for the delivery of active drugs through nasal, oral and vaginal mucosa: Current status and future perspectives. *Mater. Sci. Eng. C* **2020**, *111*, 110756.
(10) Barua, S.; Mitragotri, S. Challenges associated with Penetration of Nanoparticles across Cell and Tissue Barriers: A Review of Current Status and Future Prospects. *Nano Today* **2014**, *9*, 223−243.
(11) Zhang, H.; Zhang, J.; Streisand, J. B. Oral Mucosal Drug DeliveryClinical Pharmacokinetics and Therapeutic Applications Hao Zhang,1 Jie Zhang2 and James B. Streisand. *Clin. Pharmacokinet.* **2002**, *41*, 661−680.
(12) Shaikh, R.; Singh, T. R. R.; Garland, M. J.; Woolfson, A. D.; Donnelly, R. F. Mucoadhesive drug delivery systems. *J. Pharm. Bioallied Sci.* **2011**, *3*, 89−100.
(13) Patel, V. F.; Fang, L.; Brown, M. B. Advances in oral transmucosal drug delivery. *J. Control. Release* **2020**, *153*, 106−116.
(14) Greaves, J. L.; Wilson, C. G. Treatment of diseases of the eye with mucoadhesive delivery systems. *Adv. Drug Deliv. Rev.* **1993**, *11*, 349−383.
(15) Illangakoon, U. E.; Gill, H.; Sherman, G. C.; Parhizkar, M.; S, M.; Chatterton, N. P.; Williams, G. R. Fast dissolving paracetamol/caffeine nanofibers prepared by electrosphinning. *Int. J. Pharm.* **2014**, *477*, 369−379.
(16) Fonseca, D. F. S.; et al. Pullulan Microneedle Pathces for the efficient. *Carbohydrat. Polym.* **2020**, *241*, 116314.
(17) Vaidyaa, A.; Mitragotri, S. Ionic liquid-mediated delivery of insulin to buccal mucosa. *J. Control. Release* **2020**, *327*, 26.
(18) Wright, A. K.; Kontopantelis, E.; Emsley, R.; Buchan, I.; Sattar, N.; Rutter, M. K.; Ashcroft, D. M. Life Expectancy and Cause-Specific Mortality in Type 2 Diabetes: A Population-Based Cohort Study Quantifying Relationships in Ethnic Subgroups. *Diabetes Care* **2017**, *40*, 338−345.
(19) Pagneux, Q.; Ye, R.; Li, C.; Barras, A.; Hennuyer, N.; Staels, B.; Caina, D.; Avila Osses, J. I.; Abderrahmani, A.; Plaisance, V.; Pawlowski, V.; Boukherroub, R.; Melinte, S.; Szunerits, S. Electro-thermal patches driving the transdermal delivery of insulin. *Nanoscale Horizon* **2020**, *5*, 663−670.
(20) Teodorescu, F.; Yavuz, O.; Abderrahmani, A.; Foulon, C.; Lecoeur, M.; Sanyal, R.; Sanyal, A.; Boukherroub, R.; Szunerits, S. Photothermally triggered on-demand insulin release from reduced graphene oxide modified hydrogels. *J. Control. Release* **2017**, *246*, 164−173.
(21) Thirion-Delalande, C.; Gervais, F.; Fisch, C.; Cuiné, J.; Baron-Bodo, V.; Moingeon, P.; Mascarell, L. Comparative analysis of the oral mucosae from rodents and non-rodents: Application to the non-clinical evaluation of sublingual immunotherapy products. *PLoS One* **2017**, *12*, No. e0183398.
(22) Pinto, S.; Pintado, M. E.; Sarmento, B. In vivo,ex vivo and in vitro assessment of buccal permeation of drugs from delivery systems. *Expert Opin. Drug Delivery* **2020**, *17*, 33−48.
(23) Pillai, O.; Panchagnula, R. Polymers in Drug Delivery. *J. Control. Release* **2003**, *89*, 127.
(24) Altinbasak, I.; Jijie, R.; Barras, A.; Golba, B.; Sanyal, R.; Bouckaert, J.; Drider, D.; Bilyy, R.; Dumych, T.; Paryzhak, S.; Vovk,

V.; Boukherroub, R.; Sanyal, A.; Szunerits, S. Reduced Graphene Oxide Embedded Polymeric Nanofiber Mats: An 'On-Demand' Photothermally-Triggered Antibiotic Release Platform. *ACS Appl. Mater. Interfaces* **2018**, *10*, 41098−4110.

(25) Franz-Montan, M.; Serpe, L.; Martinelli, C. C.; da Silva, C. B.; Dos Santos, C. P.; Novaes, P. D.; Volpato, M. C.; de Paula, E.; Lopez, R. F. V.; Gropp, F. C. Evaluation of different pig oral mucosa sites as permeability barrier models for drug permeation studies. *Eur. J. Pharm. Sci.* **2016**, *81*, 52−59.

https://doi.org/10.1021/acsabm.1c01161
ACS Appl. Bio Mater. 2022, 5, 771−778